Letters

An Any-Cell-to-Any-Cell Battery Equalizer Based on Half-Bridge *LC* Converter

Fulin Liu, Runmin Zou, *Member, IEEE*, and Yonglu Liu, *Member, IEEE*

***Abstract*—This letter proposes an any-cell-to-any-cell battery equalizer based on the half-bridge *LC* converter. Cell-to-cell, cell-to-multicell, multicell-to-cell, and multicell-to-multicell balancing modes can be flexibly realized regardless of the number and location of target cells. The energy transfer between cells is controlled by modulating the fundamental harmonic voltage for each half-bridge. Meanwhile, the equalizer benefits from the resonant operation and uses the small-capacity passive components to realize lower cost and smaller size. In addition, an easy-to-realize modular structure is presented to enhance the circuit extensibility. The prototypes for five cells and three modules (nine cells) are built and tested. Experimental results confirm the validity and characteristics of the proposed equalizer.**

***Index Terms*—Any cell to any cell (AC2AC), battery string, equalizers, *LC* converter, multiwinding transformer.**

I. Introduction

ACCOMPANYING the rapid expansion of the electric vehicle (EV) market, it is anticipated that the disposal of retired lithium-ion batteries will be a new problem in the foreseeable future. Compared with the conventional material recycling solutions, the recycling of retired batteries is more economical and environmental. In fact, the retired batteries can still remain at almost 70–80% of the initial capacity, which is sufficient for safe usage in some scenarios, such as electric bicycles, low-speed EVs, and energy storage systems. However, the reassembled battery string may suffer from severe energy mismatch risk because of the different aging degrees of each recycled cell. Hence, an active battery equalizer is necessary to make the best use of recycled batteries [1].

The active equalizers can transfer energy from high-voltage cells to low-voltage ones to mitigate the energy mismatch. According to the energy balancing modes, they can be divided into five categories: adjacent cell to cell (AC2C), direct cell to cell (DC2C), cell to string (C2S), string to cell (S2C), and any-cell-to-any-cell (AC2AC). The AC2C equalizers transfer energy between adjacent cells [2], [3]. Its highlights lie in the simple structure and strong extensibility. However, several transformations are required when the target cells are far from each other. This reduces the overall efficiency, especially in the case of long battery strings [4]. The DC2C equalizers utilize selection switches to directly transfer energy from the highest voltage cell to the lowest voltage one, to some extent, improving the balancing efficiency [5]. However, numerous selection switches make the system large and complex. The C2S and S2C equalizers transfer energy between the imbalanced cell and the battery string [6], [7], [8]. Since the battery string works as a whole, some balanced cells may suffer from undesired charging or discharging. In addition, when the above equalizers balance the target cells, the other cells must wait until the target cells finish balancing. Hence, it takes a long time to balance the battery string with numerous imbalanced cells [9].

For the AC2AC equalizers, the mismatched energy is directly and simultaneously transferred from any high-voltage cells to any low-voltage ones, which realizes higher balancing flexibility [9], [10], [11], [12]. The early AC2AC equalizers remove all sensors to reduce the cost and control complexity. They operate in the fixed mode and transfer energy according to the voltage difference between cells. However, the balancing current will decrease as the voltage differences decrease, resulting in a slow overall balancing speed. In [13], a clamping structure is used to alleviate this issue. However, the balancing current under low voltage differences is still unsatisfactory. To overcome this problem, an AC2AC equalizer based on the cell voltages instead of the voltage differences is proposed in [14]. The balancing speed is greatly improved. However, to simplify the control complexity, this method only controls the balancing current direction without considering the value of the current. In addition, this method employs numerous passive components with high voltage stress and capacity to realize the low-frequency operation and capacitive isolation, making the system bulky and costly.

This letter proposes an *LC*-based AC2AC battery equalizer. It consists of a half-bridge, two resonant capacitors, a resonant inductor, and a transformer winding per cell. Owing to the resonant operation mode, the equalizer can use small-capacity passive components, realizing the compact-size structure. A fundamental modulation method applied to the half-bridge circuit

Manuscript received 5 October 2022; revised 22 November 2022; accepted 12 December 2022. Date of publication 19 December 2022; date of current version 14 February 2023. This work was supported in part by the Key R&D Program of Hunan Province of China under Grant 2020WK2007, in part by the Changsha City Science and Technology Plan Project under Grant kq2206013, and in part by Central South University Innovation-Driven Research Program under Grant 2023CXQD020. *(Corresponding authors: Runmin Zou; Yonglu Liu.)*

The authors are with the School of Automation, Central South University, Changsha 410083, China (e-mail: bxliufulin@gmail.com; runmin@gmail.com; liuyonglu@csu.edu.cn).

Color versions of one or more figures in this article are available at https://doi.org/10.1109/TPEL.2022.3230203.

Digital Object Identifier 10.1109/TPEL.2022.3230203

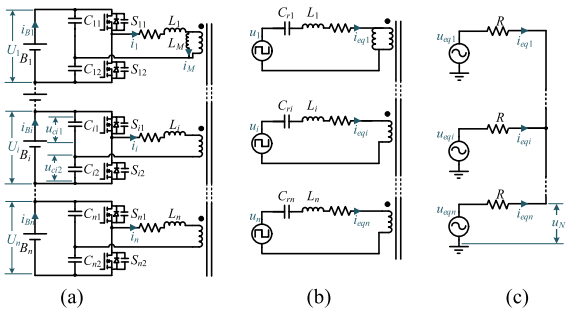

Fig. 1. Proposed AC2AC equalizer for n cells. (a) Topology structure. (b) Equivalent circuit model. (c) Simplified equivalent model.

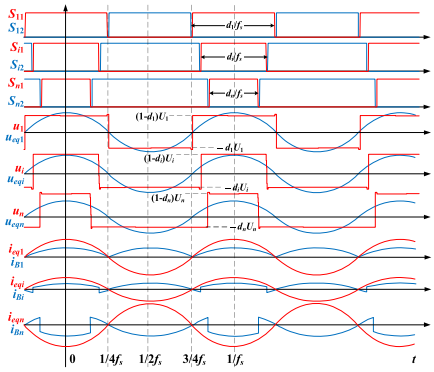

Fig. 2. Typical waveforms of the proposed equalizer.

is presented to control the energy transfer between cells. The balance between any cells can be simultaneously carried out regardless of the number and location of the target cells. Moreover, an improved modular structure is presented to enhance the circuit extensibility.

II. Proposed Battery Equalizer

A. Topology Description

The structure of the proposed equalizer is shown in Fig. 1(a). The battery cell B_i ($i = 1, 2, \ldots, n$) corresponds to a transformer winding, a half-bridge ($S_{ij}, j = 1, 2$), and a resonant tank (L_i and C_{ij}). The resonant frequency f_r of the resonant tanks is calculated as

$$f_r = 1\Big/\left(2\pi\sqrt{2LC}\right) \tag{1}$$

where L is the inductance of the inductor L_i and C is the capacitance of the capacitors C_{ij}. In addition, U_i, u_{cij}, and u_M are the terminal voltages of cell B_i, capacitor C_{ij}, and magnetizing inductor L_M, respectively. i_{Bi}, i_i, and i_M are the current of cell B_i, inductor L_i, and magnetizing inductor L_M, respectively. The number of turns of each winding is the same.

The proposed equalizer always operates at resonance, and the fundamental harmonic output of each half-bridge must be synchronized. Hence, the driving signals of the upper switches S_{i1} are in phase, and the duty cycle is defined as d_i. The driving signals of S_{i2} are complementary to that of S_{i1}. The dead time of driving signals is negligible, and the switching frequency f_s is equal to the resonant frequency f_r.

B. Operating Principles

Without loss of generality, cell B_i is taken as an example to introduce the operating principle.

Since the capacitor C_{ij} works as both a split capacitor and a resonant capacitor, its voltage u_{cij} can be expressed as

$$u_{cij} = U_{cij} + u_{rij} \tag{2}$$

where U_{cij} and u_{rij} are the dc and ac components of the voltage u_{cij}, respectively. Considering the volt–second balance principle and $U_i = u_{ci1} + u_{ci2}$, the voltages are obtained

$$U_{ci1} = (1 - d_i)\, U_i \tag{3}$$

$$U_{ci2} = d_i U_i \tag{4}$$

$$u_{ri1} = u_{ci1} - U_{ci1} = U_{ci2} - u_{ci2} = -u_{ri2}. \tag{5}$$

When switch S_{i1} is turned ON and S_{i2} is turned OFF, the following differential equations are obtained:

$$C\frac{du_{ci1}}{dt} + i_1 = C\frac{du_{ci2}}{dt} \tag{6}$$

$$L\frac{di_1}{dt} = u_{ci1} - u_M - Ri_1. \tag{7}$$

According to (2)–(5), (6) and (7) can be further rewritten as

$$C\frac{du_{ci2}}{dt} - C\frac{du_{ci1}}{dt} = 2C\frac{du_{ri2}}{dt} = i_i \tag{8}$$

$$L\frac{di_1}{dt} + u_M + Ri_1 + u_{ri2} = (1 - d_i)\, U_i. \tag{9}$$

When switch S_{i1} is turned OFF and S_{i2} is turned ON, by similar calculations, the following differential equations are obtained:

$$L\frac{di_1}{dt} + u_M + Ri_1 + u_{ri2} = -d_i U_i. \tag{10}$$

It can be seen that the difference between (9) and (10) is the polarity and value of the equivalent output voltage. From (8)–(10), an equivalent circuit is obtained, as shown in Fig. 1(b). An equivalent capacitor C_{ri} with capacitance $2C$ and voltage u_{ri2} is regarded as the resonant capacitor. The cell and switches are replaced by the voltage source u_i, which is approximated to an ideal square wave with amplitude $(1–d_i)U_i$ and $–d_iU_i$.

The typical waveform is illustrated in Fig. 2. According to the origin defined in Fig. 2, the square wave u_i can be regarded as an even function. By using Fourier transform, u_i is decomposed into cosine function, which can be expressed as

$$u_i = \sum_{k=1}^{\infty} \int_0^{1/f_r} 2f_r u_i \cos\left(2\pi k f_r t\right) dt \cos\left(2\pi k f_r t\right). \tag{11}$$

Since other harmonics make up a small proportion of the square waveform, only the fundamental harmonic is considered [9]. When $k = 1$, the fundamental harmonic $u_{\mathrm{eq}i}$ is obtained

$$u_{\mathrm{eq}i} = \frac{2U_i \sin\left(d_i\pi\right) \cos\left(2\pi f_r t\right)}{\pi}. \tag{12}$$

The amplitude of $u_{\mathrm{eq}i}$ increases with increasing d_i within $0 < d_i \leq 0.5$. When duty cycle d_i reaches 0.5, the amplitude of $u_{\mathrm{eq}i}$ reaches the maximum value $2U_i/\pi$. Hence, to facilitate the calculation, the adjustment range of duty cycles is set to 0–0.5.

At the resonant frequency f_r, the equivalent impedance of L_i and C_{ri} is equal to zero. Hence, the equivalent model can be further simplified in Fig. 1(c). R is the parasitic resistance of the circuit. The voltage of the neutral point is expressed as

$$u_N = \frac{(u_{\mathrm{eq}1} + u_{\mathrm{eq}2} + \cdots + u_{\mathrm{eq}n})}{n}. \tag{13}$$

According to Fig. 1(c), equivalent current $i_{\mathrm{eq}i}$ is expressed as

$$i_{\mathrm{eq}i} = \frac{(u_{\mathrm{eq}i} - u_N)}{R}. \tag{14}$$

Considering the impact of the half-bridge structure and duty cycle d_i, the average balancing current $i_{B\mathrm{eq}i}$ of cell B_i is obtained as

$$\begin{cases} i_{B\mathrm{eq}i} = f_r \int_0^{1/f_r} i_{Bi}dt = 4f_r \int_0^{d_i/2f_r} 0.5 i_{\mathrm{eq}i}dt \\ \qquad = \frac{2[U_i \sin(d_i\pi) - M]\sin(d_i\pi)}{R\pi^2} \\ M = \frac{[U_1 \sin(d_1\pi) + \cdots + U_n \sin(d_n\pi)]}{n} \end{cases}. \tag{15}$$

If $i_{B\mathrm{eq}i} > 0$, cell B_i releases energy; otherwise, it absorbs energy. Therefore, the balance current between cells can be controlled flexibly by adjusting the duty cycle d_i.

C. Balancing Strategy

In this letter, the equalizer adopts the open-loop balancing strategy to avoid using costly current sensors and reduce the computation burden [14]. The equalization between cells B_1, B_2, B_3, B_4, and B_5 is taken as an example to calculate the duty cycles, and other cases can be similarly analyzed. It is assumed that the cell voltages satisfy $U_1 = U_2 > U_3 > U_4 > U_5$. The calculation steps are as follows.

1) According to the voltage relationship, the energy should be delivered from B_1 and B_2 (the highest voltage cells) to B_5 (the lowest voltage cell). Hence, the expected balancing currents are set to $i_{B\mathrm{eq}1} = i_{B\mathrm{eq}2} = 0.5I_{\mathrm{set}}$, $i_{B\mathrm{eq}3} = i_{B\mathrm{eq}4} = 0$, and $i_{B\mathrm{eq}5} = -I_{\mathrm{set}}$.
2) The duty cycle first to be set is determined by the enumeration method.

First, d_1 is set to 0.5. Because $i_{B\mathrm{eq}1} = i_{B\mathrm{eq}2}$ and $U_1 = U_2$, d_2 should also be set to 0.5. According to $i_{B\mathrm{eq}1} = 0.5I_{\mathrm{set}}$, $d_1 = 0.5$, and (15), M is obtained as

$$M = U_1 \sin(d_1\pi) - \frac{\pi^2 R i_{B\mathrm{eq}1}}{2\sin(d_1\pi)} = U_1 - \frac{\pi^2 R I_{\mathrm{set}}}{4}. \tag{16}$$

Then, according to $i_{B\mathrm{eq}3} = 0$, M, and (15), duty cycles d_3 can be calculated as

$$\begin{aligned} d_3 &= \frac{\left\{\arcsin\left[\left(M + \sqrt{M^2 + 2R\pi^2 i_{B\mathrm{eq}3} U_3}\right)/2U_3\right]\right\}}{\pi} \\ &= \frac{[\arcsin(M/U_3)]}{\pi}. \end{aligned} \tag{17}$$

Similarly, d_4 and d_5 are calculated by (17). If all duty cycles can be solved, the equalizer will be controlled by these duty cycles, and steps 3 and 4 are skipped. Otherwise, step 3 should be continued.

3) Because $U_1 = U_2$, the enumeration on d_2 is skipped. For d_3 and d_4, because $i_{B\mathrm{eq}3} = i_{B\mathrm{eq}4}$, the amplitudes of $u_{\mathrm{eq}3}$ and $u_{\mathrm{eq}4}$ should be equal. Hence, we can obtain

$$2U_3 \sin(d_3\pi) = 2U_4 \sin(d_4\pi). \tag{18}$$

Considering $U_3 > U_4$, d_3 must be less than d_4. Hence, the enumeration on d_3 is also skipped. Next, d_4 is set to 0.5. M, d_1, d_2, d_3, and d_5 are calculated by the similar method of step 2. Similarly, if all duty cycles can be solved, the equalizer will be controlled by these duty cycles, and step 4 is skipped. Otherwise, step 4 should be continued.

4) d_5 is set to 0.5. M, d_1, d_2, d_3, and d_4 are calculated in turn by the similar method of step 2. If the duty cycles still cannot be solved in this step, it means that the used equivalent resistance R or the set balancing current I_{set} is too large. The circuit parameter R and the expected balancing current can be adjusted appropriately to recalculate.
5) As the equalizer operates, the cell voltage will converge gradually. Hence, after a time interval, step 1 should be restarted to recalculate the duty cycles. In addition, considering the polarization effects and nonlinear characteristics of cells, the update interval of the duty cycle can be appropriately lengthened to avoid oscillating duty cycles and unnecessary equalization progress.

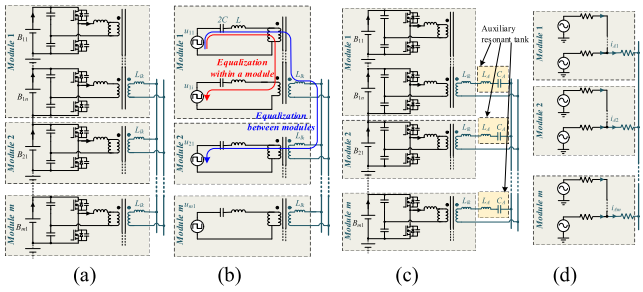

Fig. 3. Modular equalizer for m modules. (a) Conventional method [10]. (b) Equivalent model of the conventional method. (c) Proposed method. (d) Simplified circuit model of the proposed method.

D. Modular Equalization

In the practical high-power energy storage system, the number of serial cells is very large. The design difficulty of the equalizer used for a whole battery string increases sharply with increasing the cell count. Many modular equalization methods are developed to overcome this problem and improve the circuit extensibility. For the transformer-based equalizers, a conventional modular method is shown in Fig. 3(a) [10]. The circuit is equivalent in Fig. 3(b). The resonant frequency of the resonant tank between cells in different modules is changed to

$$f_{r1} = \frac{1}{\left[2\pi\sqrt{2(L + L_{\mathrm{lk}})C}\right]} \tag{19}$$

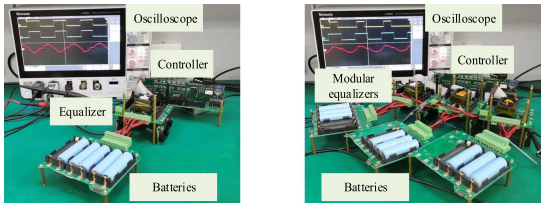

Fig. 4. Experimental prototype. (a) Equalizer for five cells. (a) Modular equalizer for nine cells (three modules).

TABLE I
EXPERIMENTAL PARAMETERS

Parameters		Value
Battery	Nominal capacity	1.5 Ah
	Nominal voltage	2.8–4.2 V
MOSFET	Model	IPA041N04NGXKSA1
Transformer	L_M	237 μH
	Leakage inductance	0.17 μH
Resonant tank	L	2.0 μH
	C	0.81 μF
Auxiliary resonant tank	L_A	1.0 μH
	C_A	3.0 μF
Resonant frequency	f_r	85 kHz
Switching frequency	f_s	84 kHz

where $L_{\rm lk}$ is the leakage inductance. The resonant frequency f_{r1} decreases with the increase of $L_{\rm lk}$. The mismatch between the resonant period and the turn-ON time results in backflow energy, which reduces the balancing performance [13].

To eliminate the effect of $L_{\rm lk}$, an auxiliary resonant tank is added to each auxiliary winding. The modular structure is presented in Fig. 3(c). The resonant frequency of the resonant tank between cells in different modules is modified to

$$f_{r2} = \frac{1}{\left[2\pi\sqrt{2\left(L + L_{\rm lk} + L_A\right)CC_A/(2C + C_A)}\right]} \tag{20}$$

where C_A is the capacitance of auxiliary capacitors and L_A is the inductance of auxiliary inductors. According to (20), the resonant frequency can be corrected to f_r by the auxiliary resonant tank. The simplified circuit model is shown in Fig. 3(d). The cells in different modules can be balanced similarly by adjusting the duty cycle. Unfortunately, the double-layer modular structure requires complex control algorithms, and the control complexity will increase with increasing the cell count.

III. EXPERIMENTAL RESULTS

Two prototypes are built to verify the feasibility of the proposed equalizer and modular structure. Fig. 4(a) shows the prototype applied to five serial lithium-ion cells (INR18650-15M). And the prototype shown in Fig. 4(b) is used to balance three modules, each consisting of three cells. Table I lists the circuit components and main parameters.

The multiwinding transformer is made by using twisted multistrand magnet copper wires. The twist process makes the windings evenly distributed, and a high spatial symmetry is realized. This coiling method helps to realize consistent windings [13]. The actual leakage inductance is near 0.17 μH. An additional

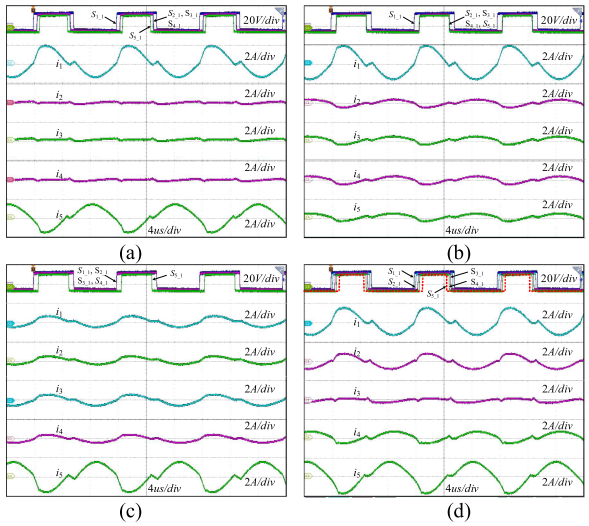

Fig. 5. Current waveforms of the resonant inductors in different cases. (a) One cell to one cell. (b) One cell to multicell. (c) Multicell to one cell. (d) Multicell to multicell.

inductance of 2 μH is connected in series to each winding. To reduce the high-frequency ac impedance and the size of passive components, the resonant frequency is set to 85 kHz. According to (1), the capacitance C is calculated at around 0.81 μF. To reduce the tolerance, three 0.27-μF capacitors are connected in parallel to replace a 0.81-μF resonant capacitor. Note that the passive components with small tolerances should be used to ensure identical resonant parameters. Considering the dead time, the switching frequency is selected to 84 kHz. The maximum balancing current is set to 0.5 A. In addition, the equivalent resistance R is measured around 70 mΩ.

Fig. 5 shows the resonant current waveforms of five resonant tanks in different cases. In Fig. 5(a), according to the amplitude and direction of the resonant currents, it can be seen that the energy is delivered from cell B_1 to B_5, and other cells are in idle. The different states of cells are adjusted by the duty cycle of each half-bridge. In Fig. 5(b) and (c), the equalizer transfers energy between a selected cell and others. In Fig. 5(d), the energy is delivered from B_1, B_2, and B_3 to B_4 and B_5. Hence, the equalizer can achieve flexible balancing modes (cell to cell, cell to multicell, multicell to cell, and multicell to multicell).

Fig. 6 shows the current waveforms of auxiliary windings with different modular structures. In Fig. 6(a) and (b), the auxiliary windings of cell-level equalizers are connected directly in parallel. In Fig. 6(c) and (d), an auxiliary structure is added to each auxiliary winding to correct the resonance parameters between modules. Compared to the waveforms of Fig. 6(a) and (b), it can be seen that the backflow energy is significantly reduced.

Fig. 7 shows the equalization results for five cells. To show the balancing performance, the initial voltage differences are set to be relatively large to simulate the bad energy mismatch. In these experiments, energy is delivered from the cells with the highest voltage to the cells with the lowest voltage. In addition, the hysteresis comparison between voltages and an update interval of 3 min are adopted to avoid oscillating duty cycles. As shown

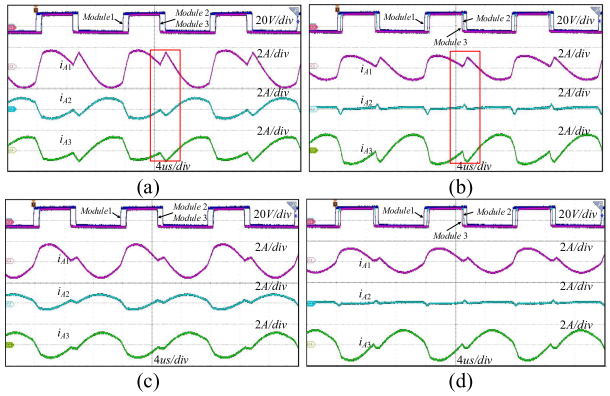

Fig. 6. Current waveforms of the auxiliary windings in different voltage conditions. (a) Case 1 without auxiliary resonant tanks. (b) Case 2 without auxiliary resonant tanks. (c) Case 1 with auxiliary resonant tanks. (d) Case 2 with auxiliary resonant tanks.

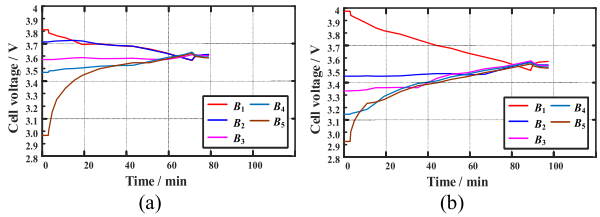

Fig. 7. Equalization results for five cells in different voltage conditions. (a) Case 1. (b) Case 2.

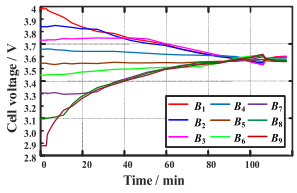

Fig. 8. Equalization results for nine cells (three modules).

in Fig. 7(a), the maximum voltage difference is reduced from 0.85 V to 20 mV. As shown in Fig. 7(b), the maximum voltage difference is reduced from 1.06 V to 60 mV. Fig. 8 shows the equalization results for three modules. The voltage difference between cells is reduced from 1.11 V to 40 mV. In practical applications, the voltage differences are much smaller due to correction in real time, resulting in a shorter balancing time. Besides, a larger balancing current can be set to accelerate the equalization.

The balancing efficiency is measured and shown in Fig. 9. A peak conversion efficiency of 92% and overall good efficiency performance are recorded. By calculating the loss breakdown, it is found that the proportion of conduction loss is obvious and increases with increasing transmission power. Hence, some methods to reduce the circuit parasitic resistance can be used to improve the efficiency.

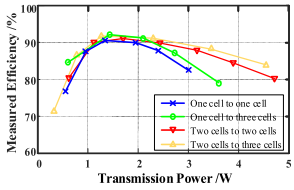

Fig. 9. Measured efficiency with respect to the transmission power.

TABLE II
COMPARISON BETWEEN EQUALIZERS IN TERMS OF COMPONENTS

Method	Cell-level equalizer				Modular structure		Cost	Size
	S*	L	C	T	L	C	($)	(cm^3)
[14]	64**	32	32	0	0	8	274	639
	30 V/9 A	30 μH	940 μF	–	–	6.6 mF	***	
Proposed equalizer	64	32	64	8	8	8	135	268
	30 V/9 A	3 μH	0.55 μF	PQ3535	2 μH	1.62 μF		

*Switch (S), Inductor (L), Capacitor (C), Transformer (T). **The component counts depend on the number of modules and cells in a battery string ($n = 4$ and $m = 8$). ***The prices are based on quantities of 1000 units using [15].

The automatic AC2AC equalizers remove sensors to reduce the cost and size [9], [10], [11], [12], [13]. However, the balancing performance under low voltage differences is unsatisfactory. In [14] and this letter, the balancing current is under control, which greatly improves the balancing speed. Compared with the equalizer of [14], the cost and size of the proposed equalizer are significantly reduced. Table II presents the comparative results in terms of the main components. To make a fair comparison, the size and cost are evaluated at the same cell voltage and balancing power [16]. Hence, the size and cost mainly depend on the number and specification of components. The comparison results show that the components of the proposed equalizer have a 50% lower cost and a 57% lower size.

IV. CONCLUSION

An AC2AC battery equalizer based on the half-bridge *LC* converter was proposed in this letter. The energy can be flexibly and directly transferred between any cells by adjusting the duty cycle for each half-bridge. To enhance the circuit extensibility, an improved modular structure was presented. The proposed equalizer benefits from the resonant operation to use compact-size passive components, compared with the existing half-bridge converter-based equalizer, reducing the cost and size of the main components by 50% and 57% separately. Finally, theoretical analysis and experimental results confirmed the validity of the proposed equalizer.

REFERENCES

[1] N. Ghaeminezhad, Q. Ouyang, X. Hu, G. Xu, and Z. Wang, "Active cell equalization topologies analysis for battery packs: A systematic review," *IEEE Trans. Ind. Electron.*, vol. 36, no. 8, pp. 9119–9135, Aug. 2021.

[2] Y. Shang, N. Cui, B. Duan, and C. Zhang, "Analysis and optimization of star-structured switched-capacitor equalizers for series-connected battery strings," *IEEE Trans. Power Electron.*, vol. 33, no. 11, pp. 9631–9646, Nov. 2018.

[3] S. Wang, S. Yang, W. Yang, and Y. Wang, "A new kind of balancing circuit with multiple equalization modes for serially connected battery pack," *IEEE Trans. Ind. Electron.*, vol. 68, no. 3, pp. 2142–2150, Mar. 2021.

[4] S. K. Dam and V. John, "Low-frequency selection switch based cell-to-cell battery voltage equalizer with reduced switch count," *IEEE Trans. Ind. Appl.*, vol. 57, no. 4, pp. 3842–3851, Jul./Aug. 2021.

[5] M. Uno and K. Yoshino, "Modular equalization system using dual phase-shift-controlled capacitively isolated dual active bridge converters to equalize cells and modules in series-connected lithium-ion batteries," *IEEE Trans. Power Electron.*, vol. 36, no. 3, pp. 2983–2995, Mar. 2021.

[6] X. Qi, Y. Wang, M. Fang, Y. Wang, and Z. Chen, "Principle and topology derivation of integrated cascade bidirectional converters for centralized charge equalization systems," *IEEE Trans. Power Electron.*, vol. 37, no. 2, pp. 1852–1869, Feb. 2022.

[7] M. Uno and A. Kukita, "String-to-battery voltage equalizer based on a half-bridge converter with multistacked current doublers for series-connected batteries," *IEEE Trans. Power Electron.*, vol. 34, no. 2, pp. 1286–1298, Feb. 2019.

[8] Z. Wei, F. Peng, and H. Wang, "An LCC-based string-to-cell battery equalizer with simplified constant current control," *IEEE Trans. Power Electron.*, vol. 37, no. 2, pp. 1816–1827, Feb. 2022.

[9] L. Liu, R. Mai, B. Xu, W. Sun, W. Zhou, and Z. He, "Design of parallel resonant switched-capacitor equalizer for series-connected battery strings," *IEEE Trans. Power Electron.*, vol. 36, no. 8, pp. 9160–9169, Aug. 2021.

[10] Y. Shang, B. Xia, C. Zhang, N. Cui, J. Yang, and C. C. Mi, "An automatic equalizer based on forward–flyback converter for series-connected battery strings," *IEEE Trans. Ind. Electron.*, vol. 64, no. 7, pp. 5380–5391, Jul. 2017.

[11] Y. Shang, N. Cui, and C. Zhang, "An optimized any-cell-to-any-cell equalizer based on coupled half-bridge converters for series-connected battery strings," *IEEE Trans. Power Electron.*, vol. 34, no. 9, pp. 8831–8841, Sep. 2019.

[12] K. Liu, Z. Yang, X. Tang, and W. Cao, "Automotive battery equalizers based on joint switched-capacitor and buck-boost converters," *IEEE Trans. Veh. Technol.*, vol. 69, no. 11, pp. 12716–12724, Nov. 2020.

[13] R. Zou, F. Liu, Y. Liu, G. Xu, and F. Liu, "An LLC-based battery equalizer with inherent current limitation," *IEEE Trans. Power Electron.*, vol. 37, no. 2, pp. 1828–1840, Feb. 2022.

[14] S. K. Dam and V. John, "A modular fast cell-to-cell battery voltage equalizer," *IEEE Trans. Power Electron.*, vol. 35, no. 9, pp. 9443–9461, Sep. 2020.

[15] Component prices as of Aug. 2022, 2022. [Online]. Available: https://www.mouser.com

[16] L. Liu et al., "A low-cost multiwinding transformer balancing topology for retired series-connected battery string," *IEEE Trans. Power Electron.*, vol. 36, no. 5, pp. 4931–4936, May 2021.